(molecular beam epitaxy) with an impurity concentration of $2 \times 10^{20}\ \mathrm{cm}^{-3}$.[2]

Experimental: The metals were deposited using e-beam evaporation with a background pressure of 2×10^{-7} T; the deposition rate (5 Å/s for Mn and 10 Å/s for Au) was regulated by a controller. Mn was deposited first followed by Au.

The specific contact resistivity was determined by the transmission-line method (TLM).[3]

Results: The influence of the Mn proportion against Au in the alloy composition on the contact resistivity has been investigated. The resulting curve is shown in Fig. 1 for an epitaxial

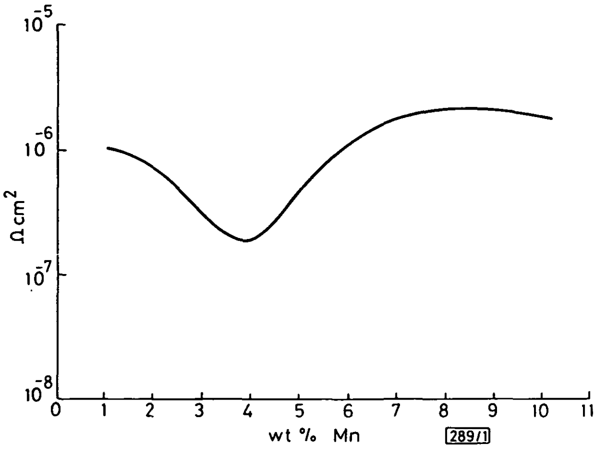

Fig. 1 *Specific contact resistivity against weight per cent of Mn*

layer with an impurity concentration of $2 \times 10^{19}\ \mathrm{cm}^{-3}$. There is a minimum of the contact resistivity ($2 \times 10^{-7}\ \Omega\mathrm{cm}^2$) at 4% Mn, but the contact resistivity is not too sensitive to the exact Mn concentration.

The alloying cycle has also been optimised. The best results are obtained with a cycle consisting of raising the temperature at 800°C/min to 400°C.

Auger spectroscopy combined with an ion-beam sputtering technique was used to analyse the in-depth diffusion of the different species. In Fig. 2 the Auger signal of each element is

Fig. 2 *Auger profile of a Au–4% Mn contact after alloying*
—— Au — — Ga ····· Mn —·— As

plotted as a function of sputtering time for a 400°C alloyed Au–4% Mn contact.

The Auger profile shows that, after alloying, Ga diffuses into the metallic film while Mn and Au move into the semiconductor. There is not any accumulation of Mn at the AuMn/GaAs interface. It is well known that the diffusion of Ga out of the semiconductor creates vacancies, and it can be thought that Mn settles into those vacancies, becoming an acceptor. However, there are other possibilities: for instance, Mn can stand in the interstitial position; however, there is not yet enough information to consolidate this.

After alloying, the surface morphology is not disturbed too much (Fig. 3). This contact is stable and the reproductibility is apparently perfect.

Very highly doped p-type layers $2 \times 10^{20}\ \mathrm{cm}^{-3}$) are very attractive for heterojunction bipolar transistors because of the reduction of the base resistance and then high-frequency potential performances. However, to obtain direct current gain the base layer must be very thin. Then this layer is easily penetrated by the metallisation junction of alloyed contacts. A nonalloyed contact is consequently required.

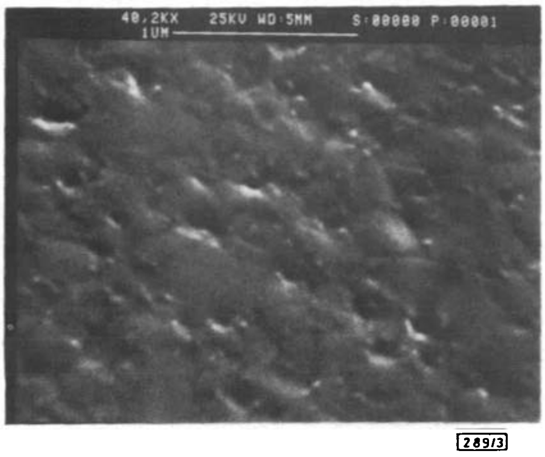

Fig. 3 *Surface morphology after alloying*

A specific contact resistivity of $2 \times 10^{-6}\ \Omega\mathrm{cm}^2$ has been obtained with a nonalloyed Au–4% Mn contact, with good reproducibility.

Conclusion: A very low-resistivity alloyed ohmic contact for p-type GaAs has been demonstrated. This alloyed contact, 4%Mn–Au, has shown impressive electrical characteristics together with good stability and reproducibility. The nonalloyed contact has also been tested for highly doped layers ($N = 2 \times 10^{20}\ \mathrm{cm}^{-3}$, $\rho = 2 \times 10^{-6}\ \Omega\mathrm{cm}$).

C. DUBON-CHEVALLIER
A. M. DUCHENOIS
J. F. BRESSE
D. ANKRI

Centre National d'Etudes des Télécommunications, PAB
Laboratoire de Bagneux
196 Rue de Paris, 92220 Bagneux, France

30th April 1985

References

1 SANADA, T., and WADA, O.: 'Ohmic contacts to p-GaAs with Au/Zn/Au structure', *Jpn. J. Appl. Phys.*, 1980, **19**, pp. L491–L494
2 LIÉVIN, J. L., and ALEXANDRE, F.: 'Ultra-high doping levels of GaAs with beryllium by molecular-beam epitaxy', *Electron. Lett.*, 1985, **21**, pp. 413–414
3 REEVES, G. K., and HARRISON, H. B.: 'Obtaining specific contact resistance from transmission line model measurements', *IEEE Electron Device Lett.*, 1982, **EDL-3**, pp. 111–113

WAVEGUIDE *E*-PLANE INTEGRATED-CIRCUIT DIPLEXER

Indexing terms: Integrated circuits, Waveguide components

A waveguide diplexer is introduced where optimised low-insertion-loss metal insert filters are directly integrated in the E-planes of the T-junction arms. The filters are designed by the exact method of field expansion into suitable eigenmodes which takes the influences of higher-order-mode interaction and finite thickness of the inserts into account. Computer optimised design data are given which provide a metal-etching technique for reliable low-cost production. Measured minimum passband insertion losses of an R120-waveguide diplexer prototype are about 0·8 dB at 10·4 GHz, and 0·5 dB at 11·2 GHz. The stopband attenuation at 10·8 GHz is about 48 dB.

Introduction: Recent advances in the design of waveguide integrated circuits have stirred the interest for reliable low-cost diplexers using printed E-plane technology.[1,2] The hitherto known constructions, however, are still based on integration of two key building blocks: channel filters and additional 3 dB couplers.[1,2] Moreover, the filters are realised only by empirical design data. It may therefore be desirable to take advantage of the full low-insertion loss, low-weight and low-cost potential inherent to this technology.[3]

This letter describes a new diplexer type (Fig. 1) where the

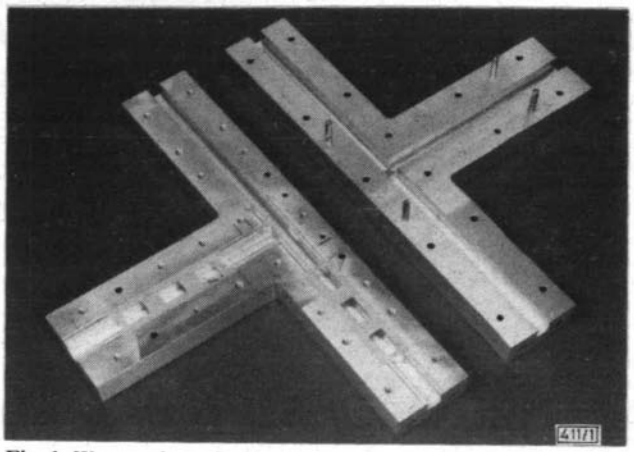

Fig. 1 *Waveguide E-plane integrated-circuit diplexer*

two E-plane filters are directly integrated in the waveguide E-plane T-junction arms. T-junction effects are compensated by suitable mechanical adjustment of the filter structure within the waveguide arms, so that no supplementary matching components are required. To avoid additional losses caused by supporting dielectrics pure metal E-plane inserts are chosen for filter elements.[3] The design of optimised low-insertion-loss metal insert filters is based on the accurate method of field expansion directly into incident and scattered waves of interest. This allows direct inclusion of both higher-order-mode coupling and finite strip thickness. The optimum low-insertion-loss filter data enable metal-etching techniques appropriate for low-cost mass production. The measured frequency response of an R120-waveguide E-plane integrated-circuit diplexer prototype shows good agreement between theory and experimental results.

Theory and design: The electromagnetic fields in each subregion at the corresponding discontinuities of the filters are derived from the x-component of the magnetic Hertzian vector,[3] which is assumed to be a sum of the eigenmodes satisfying the wave equation and the boundary conditions at the metallic surfaces:

$$\Pi_{hx} = \sum_{m=1}^{M} A_m^{\pm} T_m \sin\left[\frac{m\pi}{p} f\right] \exp(\mp jk_{zm}^2) \qquad (1)$$

where M is the number of eigenmodes considered, T_m is the normalisation factor so that the power carried by a given wave is 1 W for a wave amplitude of $1\sqrt{W}$,[3] p is the cross-section dimension[3] of the subregions under consideration, and $k_{zm}^2 = k^2 - (m\pi/p)^2$, $k^2 = \omega^2 \mu\varepsilon$.

By matching the field components at the corresponding interfaces, the coefficients $A_m^{\pm}$ in eqn. 1 are determined after multiplication with the appropriate orthogonal function.[3] This yields the scattering matrix at the step discontinuity considered. The scattering matrix of the total filter is then calculated by directly combining the single scattering matrices.

The computer-aided design is carried out by an optimisation program applying the evolution strategy method which varies the filter parameters until the desired values of the passband insertion loss and of the stopband attenuation, for given bandwidths, midband frequency and waveguide housing dimensions, are obtained. For computer optimisation, the expansion into 15 eigenmodes at each discontinuity has turned out to be sufficient. The final design data are checked up by 35 eigenmodes.

Results: An R120-waveguide diplexer for 10·4 GHz and 11·144 GHz midband frequency is chosen for design example. Fig. 2 shows the calculated insertion loss $1/|S_{21}|$ in decibels as a function of frequency for the computer-optimised E-plane integrated metal insert filters. The filters are placed in the

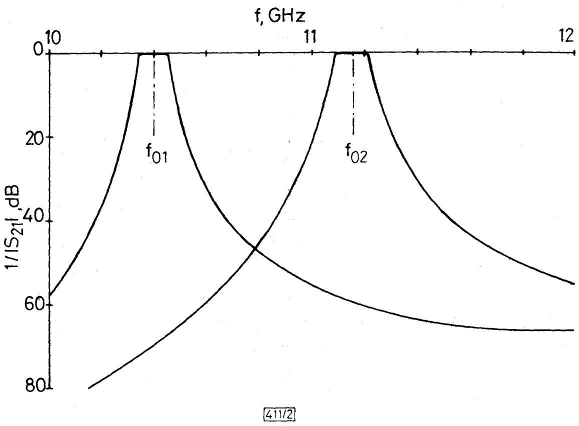

Fig. 2 *Calculated insertion loss in decibels as a function of frequency frequency*

Computer optimised design data of metal insert filters:
Metal insert thickness t = 190 μm
f_{01} = 10·4 GHz:
Metal insert lengths: 3·112 mm, 10·077 mm, 10·077 mm, 3·112 mm
Resonator lengths: 17·437 mm, 17·569 mm, 17·437 mm
f_{02} = 11·144 GHz:
Metal insert lengths: 3·331 mm, 11·210 mm, 11·210 mm, 3·331 mm
Resonator lengths: 14·319 mm, 14·415 mm, 14·319 mm

T-junction arms so as to compensate the junction effects[4] at the corresponding midband frequencies. Figs. 3 show the measured results of the constructed diplexer (Fig. 1). The minimum passband insertion losses are about 0·8 dB and 0·5 dB at 10·4 GHz and 11·2 GHz, respectively; the 3 dB bandwidths are about 130 MHz; the stopband attenuation at 10·8 GHz is about 48 dB.

Conclusion: The type of diplexer introduced utilises the full low-insertion loss, low-weight and low-cost potential inherent to the waveguide E-plane integrated-circuit technology. The channel filters are integrated directly in the T-junction wave-

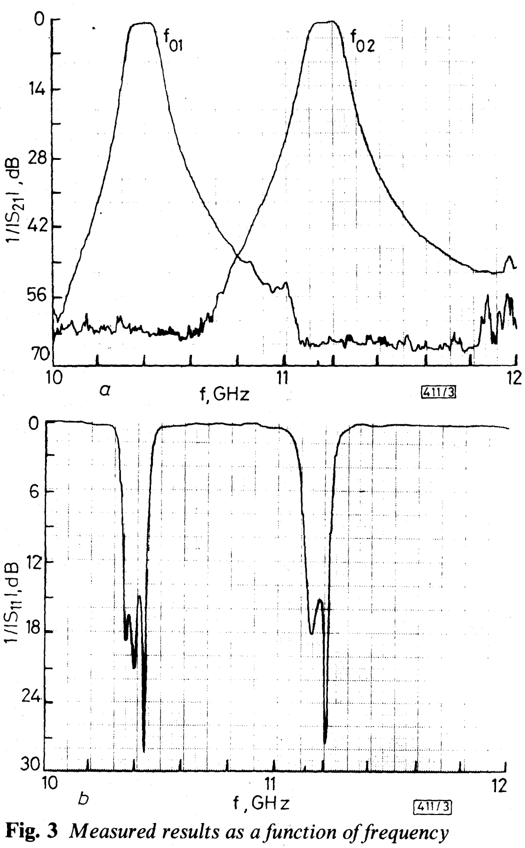

Fig. 3 *Measured results as a function of frequency*

a Insertion loss in decibels
b Return loss in decibels

guide arms and suitably placed so as to compensate the junction effects. Computer-optimised design data for optimum low-passband insertion-loss metal insert filters enable a metal-etching technique for low-cost mass production. Measured results are found to be in good agreement with the theoretically predicted values.

F. ARNDT
J. BORNEMANN
D. GRAUERHOLZ

Microwave Department
University of Bremen
Kufsteiner Str.
NW 1, D-2800 Bremen 33, W. Germany

D. FASOLD
N. SCHROEDER

Antenna Department
MBB/ERNO Raumfahrt GmbH
D-8000 München 80, W. Germany

3rd June 1985

References

1 BREUER, K., and WORONTZOFF, N.: 'A low cost multiplexer for channelized receiver front ends at millimeter waves'. 1980 IEEE MTT-S international microwave symposium digest, pp. 150–152
2 REINDEL, J.: 'Printed WG circuits trim component costs', *Microwaves*, Oct. 1980, pp. 60–63
3 VAHLDIECK, R., BORNEMANN, J., ARNDT, F., and GRAUERHOLZ, D.: 'Optimized waveguide *E*-plane metal insert filters for millimeter-wave applications', *IEEE Trans.*, 1983, **MTT-31**, pp. 65–69
4 SHARP, E. D.: 'An exact calculation for a T-junction of rectangular waveguide having arbitrary cross-section', *ibid.*, 1967, **MTT-15**, pp. 109–116

CROSSPOLARISATION DUE TO RADIAL FIELD COMPONENTS IN REFLECTOR ANTENNAS

Indexing terms: Antennas, Reflector antennas, Crosspolarisation

The letter stresses the importance of including the radial component of the transmit field of the feed horn when analysing reflector antennas. Omission of this component leads to errors in the prediction of crosspolar patterns similar in magnitude to those produced by diffraction effects within a dual reflector antenna.

Introduction: It is usual to analyse reflector antennas by the induced-current or physical optics (PO) method. Although usually requiring more computer time than, for example, the GTD, PO permits the analysis of surfaces of general shape and is, moreover, the only reliable means of predicting the co- and crosspolarised near fields of shaped reflector systems. In the PO approximation the conducting surface of a reflector is replaced by a current sheet with local electric current density $\boldsymbol{i} = 2\boldsymbol{n} \times \boldsymbol{H}_{inc}$. The use of an edge correction (e.g. through PTD) is usually unnecessary in practical antennas. However, for a precise calculation PO analyses must use the correct incident near magnetic field, and for a full-sphere solution the scattered fields of the source and reflector must be superposed.

Radial field components of a conical horn: The field transmitted by a conical feed carrying modes with $m = 1$ aximuthal symmetry can be written

$$\boldsymbol{H}_{inc} = f_1 \sin \varphi\hat{\boldsymbol{\theta}} + f_2 \cos \varphi\hat{\boldsymbol{\varphi}} + f_3 \sin \varphi\hat{\boldsymbol{r}}$$

where f_1, f_2 and f_3 are functions of r and θ. Near-field components are most efficiently calculated using a Laurent spherical-wave expansion matched to a distribution of electric and magnetic current sources on the feed aperture cap.[1,2] This method is known to provide predictions in excellent agreement with measurements. It also provides all components of the electric and magnetic fields at any point external to a 'minimum sphere' enclosing the sources.

Normalised values of H_r for two typical corrugated horns with a flare half-angle of 10° are shown in Fig. 1. The radial

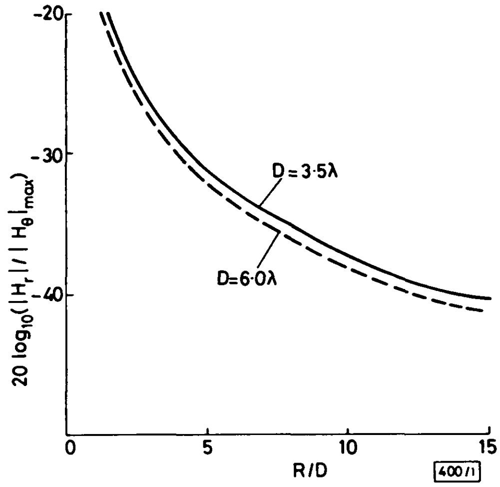

Fig. 1 *Amplitude of radial component of H relative to peak value of H_θ, for 10° flare half-angle horns*

distance R is measured in each case from the approximate far-field phase centre. H_r is essentially in phase quadrature with H_θ and H_φ for $R/D > 5{\cdot}0$, and occurs near the $-4{\cdot}6$ dB point on the copolar pattern. For large R, H_r falls off as $1/R^2$. At the traditional range of the far field $(2D^2/\lambda)$, the radial component is only -34 dB below copolar maximum for the $3{\cdot}5\lambda$ horn and -39 dB below for the 6λ horn. In addition, for the subreflector in a typical dual reflector antenna $4{\cdot}0 < R/D < 10{\cdot}0$, and the radial component lies between -30 dB and -40 dB.

Induced currents: PO induced currents resulting from the radial component of H are

$$\boldsymbol{i}' = 2f_3 \sin \varphi(n_\varphi \hat{\boldsymbol{\theta}} - n_\theta \hat{\boldsymbol{\varphi}})$$

where n_θ and n_φ are components of the unit normal to the surface in the feed co-ordinate system. For an axisymmetric

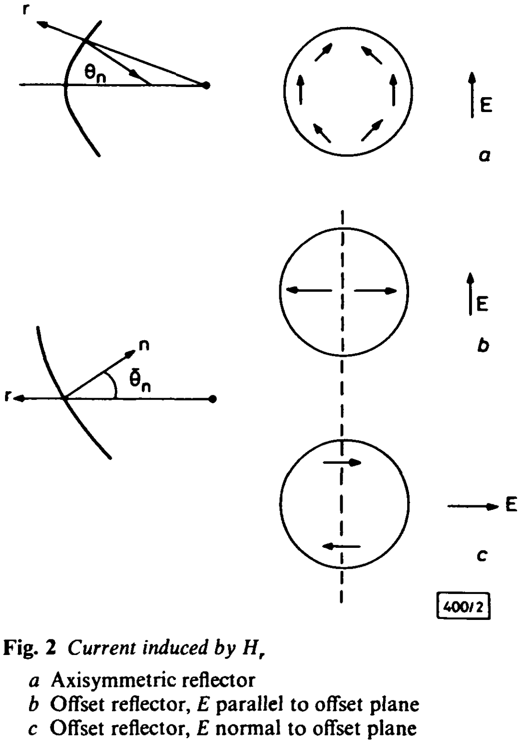

Fig. 2 *Current induced by H_r*

a Axisymmetric reflector
b Offset reflector, *E* parallel to offset plane
c Offset reflector, *E* normal to offset plane